



# DiffuseIR: Diffusion Models for Isotropic Reconstruction of 3D Microscopic Images

Mingjie Pan<sup>1</sup>, Yulu Gan<sup>2</sup>, Fangxu Zhou<sup>1</sup>, Jiaming Liu<sup>2</sup>, Ying Zhang<sup>1</sup>,  
Aimin Wang<sup>3</sup>, Shanghang Zhang<sup>2</sup>, and Dawei Li<sup>1,4(✉)</sup>

<sup>1</sup> College of Future Technology, Peking University, Beijing, China  
[lidawei@pku.edu.cn](mailto:lidawei@pku.edu.cn)

<sup>2</sup> School of Computer Science, Peking University, Beijing, China

<sup>3</sup> Department of Electronics, Peking University, Beijing, China

<sup>4</sup> Beijing Transcend Vivoscope Biotech, Beijing, China

**Abstract.** Three-dimensional microscopy is often limited by anisotropic spatial resolution, resulting in lower axial resolution than lateral resolution. Current State-of-The-Art (SoTA) isotropic reconstruction methods utilizing deep neural networks can achieve impressive super-resolution performance in fixed imaging settings. However, their generality in practical use is limited by degraded performance caused by artifacts and blurring when facing unseen anisotropic factors. To address these issues, we propose DiffuseIR, an unsupervised method for isotropic reconstruction based on diffusion models. First, we pre-train a diffusion model to learn the structural distribution of biological tissue from lateral microscopic images, resulting in generating naturally high-resolution images. Then we use low-axial-resolution microscopy images to condition the generation process of the diffusion model and generate high-axial-resolution reconstruction results. Since the diffusion model learns the universal structural distribution of biological tissues, which is independent of the axial resolution, DiffuseIR can reconstruct authentic images with unseen low-axial resolutions into a high-axial resolution without requiring re-training. The proposed DiffuseIR achieves SoTA performance in experiments on EM data and can even compete with supervised methods.

**Keywords:** Isotropic reconstruction · Unsupervised method · Diffusion model

## 1 Introduction

Three-dimensional (3D) microscopy imaging is crucial in revealing biological information from the nanoscale to the microscale. Isotropic high resolution across

---

M. Pan and Y. Gan—Equal contribution.

---

**Supplementary Information** The online version contains supplementary material available at [https://doi.org/10.1007/978-3-031-43999-5\\_31](https://doi.org/10.1007/978-3-031-43999-5_31).

all dimensions is desirable for visualizing and analyzing biological structures. Most 3D imaging techniques have lower axial than lateral resolution due to physical slicing interval limitation or time-saving consideration [8, 18, 23, 28, 31]. Effective isotropic super-resolution algorithms are critical for high-quality 3D image reconstructions, such as electron microscopy and fluorescence microscopy.

Recently, deep learning methods have made significant progress in image analysis [9, 13, 14, 25]. To address the isotropic reconstruction problem, [9] employs isotropic EM images to generate HR-LR pairs at axial and train a super-resolution model in a supervised manner, demonstrating the feasibility of inferring HR structures from LR images. [29, 30] use 3D point spread function (PSF) as a prior for self-supervised super-resolution. However, isotropic high-resolution images or 3D point spread function (PSF) physical priors are difficult to obtain in practical settings, thus limiting these algorithms. Some methods like [3, 21] have skillfully used cycleGAN [32] architecture to train axial super-resolution models without depending on isotropic data or physical priors. They learn from unpaired matching between high-resolution 2D slices in the lateral plane and low-resolution 2D slices in the axial plane, achieving impressive performance. However, these methods train models in fixed imaging settings and suffer from degraded performance caused by artifacts and blurring when facing unseen anisotropic factors. This limits their generality in practice [6]. In conclusion, a more robust paradigm needs to be proposed. Recently, with the success of the diffusion model in the image generation field [4, 11, 17, 19, 26], researchers applied the diffusion model to various medical image generation tasks and achieved impressive results [1, 12, 20, 22, 25]. Inspired by these works, we attempt to introduce diffusion models to address the isotropic reconstruction problem.

This paper proposes DiffuseIR, an unsupervised method based on diffusion models, to address the isotropic reconstruction problem. Unlike existing methods, DiffuseIR does not train a specific super-resolution model from low-axial-resolution to high-axial-resolution. Instead, we pre-train a diffusion model  $\epsilon_\theta$  to learn the structural distribution  $p_\theta(X_{lat})$  of biological tissue from lateral microscopic images  $X_{lat}$ , which resolution is naturally high. Then, as shown in Fig. 1, we propose a Sparse Spatial Condition Sampling (SSCS) to condition the reverse-diffusion process of  $\epsilon_\theta$ . SSCS extracts sparse structure context from low-axial-resolution slice  $x_{axi}$  and generate reconstruction result  $x_0 \sim p_\theta(X_{lat}|x_{axi})$ . Since  $\epsilon_\theta$  learns the universal structural distribution  $p_\theta$ , which is independent of the axial resolution, DiffuseIR can leverage the flexibility of SSCS to reconstruct authentic images with unseen anisotropic factors without requiring re-training. To further improve the quality of reconstruction, we propose a Refine-in-loop strategy to enhance the authenticity of image details with fewer sampling steps.

To sum up, our contributions are as follows:

- (1) We are the first to introduce diffusion models to isotropic reconstruction and propose DiffuseIR. Benefiting from the flexibility of SSCS, DiffuseIR is naturally robust to unseen anisotropic spatial resolutions.
- (2) We propose a Refine-in-loop strategy, which maintains performance with fewer sampling steps and better preserves the authenticity of the reconstructed image details.
- (3) We perform extensive experiments on EM data with different imaging settings

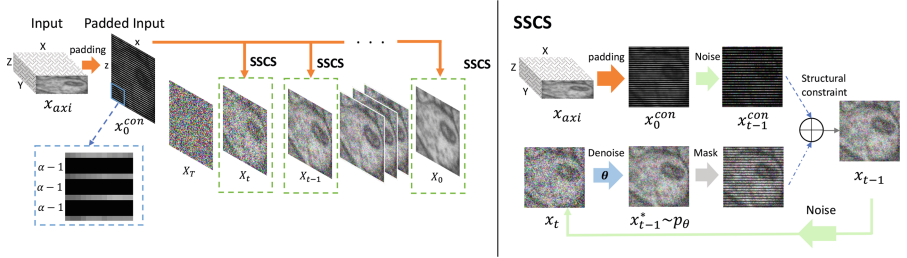


**Fig. 1. Method Pipeline.** DiffuseIR progressively conditions the denoising process with SSCS. For SSCS, we perform intra-row padding on input  $X_{lat}$  using the anisotropy factor  $\alpha$  to obtain spatially aligned structural context, which is then merged with the diffusion model's output. Iterative SSCS refines reconstruction.

and achieve SOTA performance. Our unsupervised method is competitive with supervised methods and has much stronger robustness.

## 2 Methodology

As shown in Fig. 1, DiffuseIR address isotropic reconstruction by progressively conditions the denoising process of a pre-trained diffusion model  $\epsilon_\theta$ . Our method consists of three parts: DDPM pre-train, Sparse Spatial Condition Sampling and Refine-in-loop strategy.

**DDPM Pretrain on Lateral.** Our method differs from existing approaches that directly train super-resolution models. Instead, we pre-train a diffusion model to learn the distribution of high-resolution images at lateral, avoiding being limited to a specific axial resolution. Diffusion models [10, 19] employ a Markov Chain diffusion process to transform a clean image  $x_0$  into a series of progressively noisier images during the forward process. This process can be simplified as:

$$q(x_t|x_0) = N(x_t; \sqrt{\bar{\alpha}_t}x_0, (1 - \bar{\alpha}_t)I), \quad (1)$$

where  $\bar{\alpha}_t$  controls the scale of noises. During inference, the model  $\epsilon_\theta$  predicts  $x_{t-1}$  from  $x_t$ . A U-Net  $\epsilon_\theta$  is trained for denoising process  $p_\theta$ , which gradually reverses the diffusion process. This denoising process can be represented as:

$$p_\theta(x_{t-1}|x_t) = N(x_{t-1}; \epsilon_\theta(x_t, t), \sigma_t^2 I), \quad (2)$$

During training, we use 2D lateral slices, which is natural high-resolution to optimize  $\epsilon_\theta$  by mean-matching the noisy image obtained in Eq. 1 using the MSE loss [10]. Only HR slices at lateral plane  $X_{lat}$  were used for training, so the training process is unsupervised and independent of the specific axial resolution. So that  $\epsilon_\theta$  learns the universal structural distribution of biological tissues and can generate realistic HR images following  $p_\theta(X_{lat})$ .

**Sparse Spatial Condition Sampling on Axial.** We propose Sparse Spatial Condition Sampling (SSCS) to condition the generation process of  $\epsilon_\theta$  and generate high-axial-resolution reconstruction results. SSCS substitutes every reverse-diffusion step Eq. 2. We first transform the input axial LR slice  $x_{axi}$  to match the lateral resolution by intra-row padding:  $(\alpha - 1)$  rows of zero pixels are inserted between every two rows of original pixels, where  $\alpha$  is the anisotropic spatial factor. We denote  $M$  as the mask for original pixels in  $x_0^{con}$ , while  $(1 - M)$  represents those empty pixels inserted. In this way, we obtain  $x_0^{con}$ , which reflects the sparse spatial content at axial, and further apply Eq. 1 to transform noise level:

---

**Algorithm 1:** Isotropic reconstruction using basic DiffuseIR

---

```

Input: axial slice  $x_{axi}$ , anisotropic factor  $\alpha$ , refine-in-loop counts  $K$ 
1  $x_0^{con}, M \leftarrow padding(x_{axi}, \alpha)$ 
2 for  $t = T, \dots, 1$  do
3    $x_{t-1}^{con} \sim N(\sqrt{\alpha_t}x_0^{con}, (1 - \bar{\alpha}_t)I)$ 
4   for  $i = 1, \dots, K$  do
5      $x_{t-1}^* \sim N(x_{t-1}; \epsilon_\theta(x_t, t), \sigma_t^2 I)$ 
6      $x_{t-1} = M * x_{t-1}^{con} + (1 - M) * x_{t-1}^*$ 
7     if  $t > 1$  and  $i < K$  then
8        $| x_t \sim N(\sqrt{1 - \beta_t}x_{t-1}, \beta_t I)$ 
9     end
10   end
11 end
12 return  $x_0$ 

```

---

$$x_{t-1}^{con} \sim N(\sqrt{\alpha_t}x_0^{con}, (1 - \bar{\alpha}_t)I) \quad (3)$$

Then, SSCS sample  $x_{t-1}$  at any time step  $t$ , conditioned on  $x_{t-1}^{con}$ . The process can be described as follows:

$$x_{t-1} = M \odot x_{t-1}^{con} + (1 - M) \odot x_{t-1}^* \quad (4)$$

where  $x_{t-1}^*$  is obtained by sampling from the model  $\epsilon_\theta$  using Eq. 2, with  $x_t$  of the previous iteration.  $x_{t-1}^*$  and  $x_{t-1}^{con}$  are combined with  $M$ . By iterative denoising, we obtain the reconstruction result  $x_0$ . It conforms to the distribution  $p_\theta(X_{lat})$  learned by the pre-trained diffusion model and maintains semantic consistency with the input LR axial slice. Since SSCS is parameter-free and decoupled from the model training process, DiffuseIR can adapt to various anisotropic spatial resolutions by modifying the padding factor according to  $\alpha$  while other methods require re-training. This makes DiffuseIR a more practical and versatile solution for isotropic reconstruction.

**Refine-in-Loop Strategy.** We can directly use SSCS to generate isotropic results, but the reconstruction quality is average. The diffusion model is capable of extracting context from the sparse spatial condition. Still, we have discovered a phenomenon of texture discoordination at the mask boundaries, which reduces the reconstruction quality. For a certain time step  $t$ , the content of  $x_{t-1}^*$  may be unrelated to  $x_{t-1}^{con}$ , resulting in disharmony in  $x_{t-1}$  generated by SSCS. During the denoising of the next time step  $t-1$ , the model tries to repair the disharmony of  $x_{t-1}$  to conform to  $p_\theta$  distribution. Meanwhile, this process will introduce new inconsistency and cannot converge on its own. To overcome this problem, we propose the Refine-in-loop strategy: For  $x_{t-1}$  generated by SSCS at time step  $t$ , we apply noise to it again and obtain a new  $x_t$  and then repeat SSCS at time step  $t$ . Our discovery showed that this uncomplicated iterative refinement method addresses texture discoordination significantly and enhances semantic precision.

The total number of inference steps in DiffuseIR is given by  $T_{total} = T \cdot K$ . As  $T_{total}$  increases, it leads to a proportional increase in the computation time of our method. However, larger  $T_{total}$  means more computational cost. Recent works such as [15, 16, 24] have accelerated the sampling process of diffusion models by reducing  $T$  while maintaining quality. For DiffuseIR, adjusting the sampling strategy is straightforward. Lowering  $T$  and raising refinement iterations  $K$  improves outcomes with a fixed  $T_{total}$ . We introduce and follow the approach presented in DDIM [24] as an example and conducted detailed ablation experiments in Sec. 3 to verify this. Our experiments show that DiffuseIR can benefit from advances in the community and further reduce computational overhead in future work.

### 3 Experiments and Discussion

**Dataset and Implement Details.** To evaluate the effectiveness of our method, we conducted experiments on two widely used public EM datasets, FIB-25 [27] and Cremi [5]. FIB-25 contains isotropic drosophila medulla connectome data obtained with FIB-SEM. We partitioned it into subvolumes of  $256 \times 256 \times 256$  as ground truth and followed [9] to perform average-pooling by factor  $\alpha(x2, x4, x8)$  along the axis to obtain downsampled anisotropic data. Cremi consists of drosophila brain data with anisotropic spatial resolution. We followed [3] to generate LR images with a degradation network and conduct experiments on lateral slices. All resulting images were randomly divided into the training (70%), validation (15%) and test (15%) set. For the pre-training of the diffusion model, we follow [19] by using U-Net with multi-head attention and the same training hyper-parameters. We use  $256 \times 256$  resolution images with a batch size of 4 and train the model on  $8 \times$ V100 GPUs. For our sampling setting, we set  $T, K = 25, 40$ , which is a choice selected from the ablation experiments in Sec. 3 that balances performance and speed.

**Quantitative and Visual Evaluation.** To evaluate the effectiveness of our method, we compared DiffuseIR with SoTA methods and presented the quantitative results in Table 1. We use PSNR and SSIM to evaluate results. PSNR is calculated using the entire 3D stack. SSIM is evaluated slice by slice in XZ and YZ viewpoints, with scores averaged for the final 3D stack score, measuring quality and 3D consistency. We use cubic interpolation as a basic comparison. 3DSRUNet [9] is a seminal isotropic reconstruction method, which requires HR and LR pairs as ground truth for supervised training. CycleGAN-IR [3] proposed an unsupervised approach using a CycleGAN [32] architecture, learning from unpaired axial and lateral slices. These methods train specialized models for a fixed anisotropic spatial setting and must be retrained for unseen anisotropic factors  $\alpha$ , shown in Table 1. Despite being trained solely for denoising task and not exposed to axial slices, DiffuseIR outperforms unsupervised baselines and is competitive with supervised methods [9]. As shown in Fig. 2, our refine-in-loop strategy produces results with greater visual similarity to the Ground Truth, avoiding distortion and blurriness of details. Notably, the versatility afforded by

**Table 1. Quantitative evaluation of DiffuseIR against baselines.** PSNR↑ and SSIM↑ are used as evaluation metrics. We evaluated the FIB25 and Cremi datasets, considering three anisotropic spatial resolutions,  $\alpha = 2, 4, 8$ . Unlike other baselines which train a dedicated model for each  $\alpha$ , our method only trains a single, generalizable model.

Methzod		FIB25			Cremi		
		$\times 2$	$\times 4$	$\times 8$	$\times 2$	$\times 4$	$\times 8$
Interpolation	PSNR	33.21	30.29	29.19	31.44	29.34	28.27
	SSIM	0.854	0.722	0.538	0.782	0.574	0.451
†3DSRUNet	PSNR	<b>33.84</b>	32.31	30.97	<b>32.04</b>	31.12	<b>30.28</b>
	SSIM	0.877	0.824	0.741	<b>0.820</b>	0.761	0.719
CycleGAN-IR	PSNR	33.54	31.77	29.94	31.71	30.47	29.04
	SSIM	0.869	0.798	0.640	0.794	0.721	0.560
<b>DiffuseIR (ours)</b>	PSNR	33.81	<b>32.37</b>	<b>31.09</b>	31.97	<b>31.24</b>	30.24
	SSIM	<b>0.881</b>	<b>0.832</b>	<b>0.774</b>	0.819	<b>0.783</b>	<b>0.726</b>

† Supervised method.

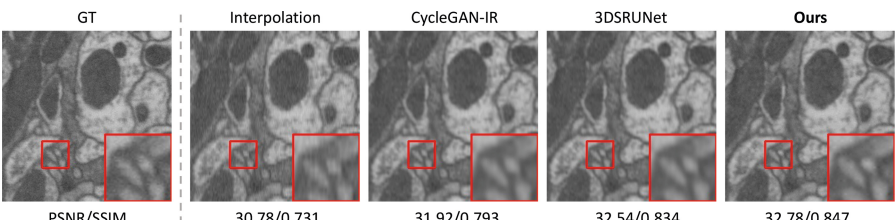


**Fig. 2. Visual comparisons on FIB-25 dataset ( $\alpha = 4$ ).** DiffuseIR can generate competitive results compared to supervised methods, and the results appear more visually realistic.

CycleGAN-IR	3DSRUNet	DiffuseIR(Ours)	CycleGAN-IR	3DSRUNet	DiffuseIR(Ours)	GT
FIB25, $\alpha=4 \rightarrow \alpha=8$						
30.21/0.677	30.95/0.738	<b>32.10/0.822</b>	32.04/0.821	32.71/0.838	<b>33.17/0.856</b>	
Cremi, $\alpha=4 \rightarrow \alpha=8$						
29.68/0.633	30.66/0.734	<b>31.17/0.768</b>	30.56/0.717	31.34/0.792	<b>31.78/0.820</b>	
(a)			(b)			

**Fig. 3. Analysis on robustness.** (a) Test on unseen anisotropic factor  $\alpha$ . (b) Test on different datasets with domain shifts (e.g., train on FIB25, test on Cremi). Our method is robust against various anisotropic factors and domain shifts between two datasets.

SSCS allows DiffuseIR to achieve excellent results using only one model, even under different isotropic resolution settings. This indicates that DiffuseIR overcomes the issue of generalization to some extent in practical scenarios, as users no longer need to retrain the model after modifying imaging settings.

**Further Analysis on Robustness.** We examined the robustness of our model to variations in both Z-axis resolutions and domain shifts. Specifically, we investigated the following: **(a) Robustness to unseen anisotropic spatial factors.** The algorithm may encounter unseen anisotropic resolution due to the need for different imaging settings in practical applications. To assess the model's robustness to unseen anisotropic factors, we evaluated the model trained with the anisotropic factor  $\alpha = 4$ . Then we do inference under the scenario of anisotropic factor  $\alpha = 8$ . For those methods with a fixed super-resolution factor, we use cubic interpolation to upsample the reconstructed result by 2x along the axis. **(b) Robustness to the domain shifts.** When encountering unseen data in the real world, domain shifts often exist, such as differences in biological structure features and physical resolution, which can impact the model's performance [2, 7]. To evaluate the model's ability to handle those domain shifts, we trained our model on one dataset and tested it on another dataset. **Analysis:** As shown in Fig. 3, DiffuseIR shows greater robustness than other methods. In scenario **(a)**, other methods are trained on specific anisotropic factors for super-resolution of axial LR to lateral HR. This can result in model fragility during testing with unseen anisotropic resolutions. In contrast, DiffuseIR directly learns the universal structural distribution at lateral through generation task, applicable to various axial resolutions. All methods exhibit decreased performance in scenario **(b)**. However, DiffuseIR shows a small performance degradation with the help of the multi-step generation of the diffusion model and sparse spatial constraints imposed by SSCS at each reverse-diffusion step. Further, compared to the pre-

vious methods predicting the result by one step, DiffuseIR makes the generating process more robust and controllable by adding constraints at each step to prevent the model from being off-limit.

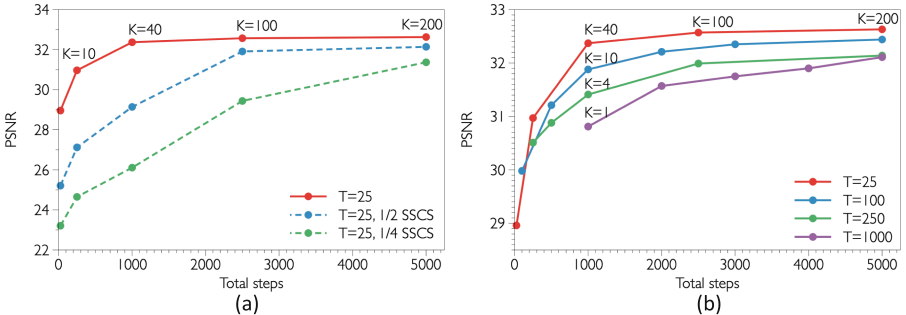


**Fig. 4. Ablation Study:** (a) ablation on SSCS frequency. Experimental results demonstrates the importance of SSCS. When reducing the frequency of SSCS usage, performance will severely decline. (b) ablation on different refine-in-loop settings. The results show that when the number of total steps is fixed, increase K will lead to higher PSNR.

**Ablation Study.** We conducted extensive ablation experiments Fig. 4. First, to demonstrate the effectiveness of SSCS, we use it only in partially alternate reverse-diffusion steps, such as 1/4 or 1/2 steps. As shown in Fig. 4 (a), increasing the frequency of SSCS significantly improves PSNR while bringing negligible additional computational costs. This indicates that SSCS have a vital effect on the model’s performance. Second, for the Refine-in-loop strategy, results show that keeping the total number of steps unchanged (reducing the number of time steps  $T$  while increasing the refine iterations  $K$ ) can markedly improve performance. Figure 4 (b) have the following settings:  $T = \{25, 100, 250, 1000\}$  with  $K \{40, 10, 4, 1\}$  to achieve a total of 5000 steps. The results show that the model performs best when  $T = 25$  and PSNR gradually increases with the increase of  $K$ . A balanced choice is  $\{T = 25, K = 40\}$ , which improves PSNR by 1.56dB compared to  $\{T = 1000, K = 1\}$  without using the Refine-in-loop strategy.

## 4 Conclusion

We introduce DiffuseIR, an unsupervised method for isotropic reconstruction based on diffusion models. To the best of our knowledge, We are the first to introduce diffusion models to solve this problem. Our approach employs Sparse Spatial Condition Sampling (SSCS) and a Refine-in-loop strategy to generate results robustly and efficiently that can handle unseen anisotropic resolutions. We evaluate DiffuseIR on EM data. Experiments results show our methods achieve SoTA methods and yield comparable performance to supervised methods. Additionally, our approach offers a novel perspective for addressing Isotropic Reconstruction problems and has impressive robustness and generalization abilities.

## 5 Limitation

DiffuseIR leverages the powerful generative capabilities of pre-trained Diffusion Models to perform high-quality isotropic reconstruction. However, this inevitably results in higher computational costs. Fortunately, isotropic reconstruction is typically used in offline scenarios, making DiffuseIR’s high computational time tolerable. Additionally, the community is continuously advancing research on accelerating Diffusion Model sampling, from which DiffuseIR can benefit.

**Acknowledgments.** The authors acknowledge supports from Beijing Nova Program and Beijing Transcend Vivoscope Biotech Co., Ltd.

## References

- Chung, H., Chul Ye, J.: Score-based diffusion models for accelerated MRI. *Med. Image Anal.* **80**, 102479 (2023)
- Csurka, G.: Domain adaptation for visual applications: a comprehensive survey. *arXiv: Computer Vision and Pattern Recognition* (2017)
- Deng, S., et al.: Isotropic reconstruction of 3D EM images with unsupervised degradation learning. In: Martel, A.L., et al. (eds.) *MICCAI 2020*. LNCS, vol. 12265, pp. 163–173. Springer, Cham (2020). [https://doi.org/10.1007/978-3-030-59722-1\\_16](https://doi.org/10.1007/978-3-030-59722-1_16)
- Dhariwal, P., Nichol, A.: Diffusion models beat GANs on image synthesis. In: *Neural Information Processing Systems* (2021)
- Funke, J., S.: *cremi.org*. <http://cremi.org/>
- González-Ruiz, V., García-Ortiz, J., Fernández-Fernández, M., Fernández, J.J.: Optical flow driven interpolation for isotropic FIB-SEM reconstructions. *Comput. Meth. Programs Biomed.* **221**, 106856 (2022)
- Guan, H., Liu, M.: Domain adaptation for medical image analysis: a survey (2021)
- Hayworth, K.J., et al.: Ultrastructurally smooth thick partitioning and volume stitching for large-scale connectomics. *Nat. Methods* **12**, 319–322 (2015)
- Heinrich, L., Bogovic, J.A., Saalfeld, S.: Deep learning for isotropic super-resolution from non-isotropic 3d electron microscopy. *medical image computing and computer assisted intervention* (2017)
- Ho, J., Jain, A., Abbeel, P.: Denoising diffusion probabilistic models. In: *Neural Information Processing Systems* (2020)
- Kawar, B., Elad, M., Ermon, S., Song, J.: Denoising diffusion restoration models (2023)
- Kim, B., Chul, J.: Diffusion deformable model for 4d temporal medical image generation. In: Wang, L., Dou, Q., Fletcher, P.T., Speidel, S., Li, S. (eds.) *MICCAI 2022*. LNCS, vol. 13431, pp. 539–548. Springer, Cham (2023). [https://doi.org/10.1007/978-3-031-16431-6\\_51](https://doi.org/10.1007/978-3-031-16431-6_51)
- Li, X., et al.: Efficient meta-tuning for content-aware neural video delivery. In: Avidan, S., Brostow, G., Cissé, M., Farinella, G.M., Hassner, T. (eds.) *ECCV 2022*. LNCS, vol. 13678, pp. 308–324. Springer, Cham (2022). [https://doi.org/10.1007/978-3-031-19797-0\\_18](https://doi.org/10.1007/978-3-031-19797-0_18)
- Liu, J., et al.: Overfitting the data: compact neural video delivery via content-aware feature modulation. In: *2021 IEEE/CVF International Conference on Computer Vision (ICCV)* (2021). <https://doi.org/10.1109/iccv48922.2021.00459>

15. Lu, C., Zhou, Y., Bao, F., Chen, J., Li, C., Zhu, J.: DPM-solver: a fast ode solver for diffusion probabilistic model sampling in around 10 steps (2022)
16. Lu, C., Zhou, Y., Bao, F., Chen, J., Li, C., Zhu, J.: Dpm-solver++: fast solver for guided sampling of diffusion probabilistic models (2022)
17. Lugmayr, A., Danelljan, M., Romero, A., Yu, F., Timofte, R., Gool, L.V.: Repaint: inpainting using denoising diffusion probabilistic models (2023)
18. Mikula, S.: Progress towards mammalian whole-brain cellular connectomics. *Front. Neuroanat.* **10**, 62 (2016)
19. Nichol, A., Dhariwal, P.: Improved denoising diffusion probabilistic models. arXiv: Learning (2021)
20. Özbey, M., et al.: Unsupervised medical image translation with adversarial diffusion models (2022)
21. Park, H., et al.: Deep learning enables reference-free isotropic super-resolution for volumetric fluorescence microscopy. *Nature Commun.* **13**, 3297 (2021)
22. Peng, C., Guo, P., Zhou, S.K., Patel, V., Chellappa, R.: Towards performant and reliable undersampled MR reconstruction via diffusion model sampling (2023)
23. Schrödel, T., Prevedel, R., Aumayr, K., Zimmer, M., Vaziri, A.: Brain-wide 3d imaging of neuronal activity in *caenorhabditis elegans* with sculpted light. *Nat. Meth.* **10**, 1013–1020 (2013)
24. Song, J., Meng, C., Ermon, S.: Denoising diffusion implicit models. arXiv: Learning (2020)
25. Song, Y., Shen, L., Xing, L., Ermon, S.: Solving inverse problems in medical imaging with score-based generative models. Cornell University - arXiv (2021)
26. Su, X., Song, J., Meng, C., Ermon, S.: Dual diffusion implicit bridges for image-to-image translation (2023)
27. ya Takemura, S., et al.: Synaptic circuits and their variations within different columns in the visual system of drosophila. In: *Proceedings of the National Academy of Sciences of the United States of America* (2015)
28. Verveer, P.J., Swoger, J., Pampaloni, F., Greger, K., Marcello, M., Stelzer, E.H.K.: High-resolution three-dimensional imaging of large specimens with light sheet-based microscopy. *Nat. Methods* **4**, 311–313 (2007)
29. Weigert, M., Royer, L., Jug, F., Myers, G.: Isotropic reconstruction of 3D fluorescence microscopy images using convolutional neural networks. arXiv: Computer Vision and Pattern Recognition (2017)
30. Weigert, M., et al.: Content-aware image restoration: pushing the limits of fluorescence microscopy. *bioRxiv* (2018)
31. Wu, Y., et al.: Three-dimensional virtual refocusing of fluorescence microscopy images using deep learning. *Nature Methods* **16**, 1323–1331 (2019)
32. Zhu, J.Y., Park, T., Isola, P., Efros, A.A.: Unpaired image-to-image translation using cycle-consistent adversarial networks. In: *International Conference on Computer Vision* (2017)